Supplemental Material

Area codes

Figure S1 displays the 47 area codes and their boundaries and Table S1 provides the information in tabular format.

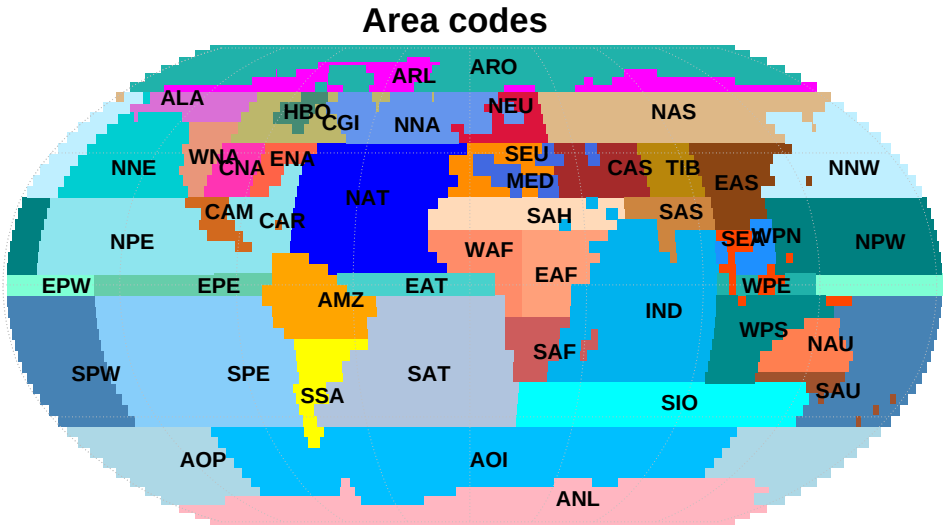

Figure S1: Area codes.

Table S1: Climate Region Definition.

Code	Full name	Zone	Latitude	Longitude	Type
ARL	Arctic Land	North	67.5 90	-180 180	l
ARO	Arctic Ocean	North	67.5 90	-180 180	o
ANL	Antarctic Land	South	-90 -55	-180 180	l
AOP	Antarctic Ocean Pacific	South	-90 -50	120 250	o
AOI	Antarctic Ocean Indian	South	-90 -50	-10 120	o
ALA	Alaska	North	57.5 67.5	-170 -105	l
CGI	East Canada Greenland And Iceland	North	50 67.5	-105 -10	l
WNA	West North America	Mid-N	30 57.5	-135 -105	l
CNA	Central North America	Mid-N	30 50	-105 -85	l
ENA	East North America	Mid-N	30 50	-85, -50	l
CAM	Central AMerica	Mid-N	10 30	-115 -70	l
AMZ	Amazonia	Mid-S	-20 10	-82.5 -30	l
SSA	South South America	Mid-S	-55 -20	-75 -30	l
NEU	North EUrope	North	47.5 67.5	-10 40	l
SEU	South EUrope	Mid-N	30 47.5	-10 40	l
SAH	SAHara	Mid-N	17.5 30	-20 65	l
WAF	West AFrica	Equat	-10 17.5	-20 25	l
EAF	East AFrica	Equat	-10 17.5	25, 60	l
SAF	South AFrica	Mid-S	-35 -10	10 60	l
NAS	North ASia	North	50 67.5	40 190	l
CAS	Centra ASia	Mid-N	30 50	40 75	l
TIB	TIBet	Mid-N	30 50	75 100	l
EAS	East ASia	Mid-N	20 50	100 150	l
SAS	South ASia	Mid-N	5 30	65 100	l
SEA	South East Asia	Equat	-10 20	100 150	l
NAU	North AUstralia	Mid-S	-30 -10	110 155	l
SAU	South AUstralia	Mid-S	-47.5 -30	110 180	l
MED	MEDiterranean	Mid-N	30 50	2.5 70	o
CAR	CARibbean	Mid-N	5 50	-95 -65	o
IND	INDian ocean	Equat	-35 30	25 100	o
SPW	South Pacific West	Mid-S	-50 -5	145 220	o
SPE	South Pacific East	Mid-S	-50 -5	-140 -65	o
EPW	Equatorial Pacific West	Equat	-5 5	137.5, 220	o
EPE	Equatorial Pacific East	Equat	-5 5	-140 -70	o
NPW	North Pacific West	Mid-N	5 30	120 195	o
NPE	North Pacific East	Mid-N	5 30	-165 -95	o
NAT	North ATlantic	Mid-N	5 50	-65 2.5	o
SAT	South ATlantic	Mid-S	-50 -5	-65 25	o
EAT	Equatorial ATlantic	Equat	-5 5	-65 25	o
SIO	South Indian Ocean	Mid-S	-50 -35	25 145	o
NNE	North North East pacific	North	30 67.5	-165 -105	o
NNW	North North West pacific	North	30 67.5	100 195	o
WPE	Warm Pool Equatorial	Equat	-5 5	100 137.5	o
WPS	Warm Pool South	Mid-S	-35 -5	100 145	o
HBO	Hudson Bay Ocean	North	50 67.5	-95 -70	o
WPN	Warm Pool North	Mid-N	5 30	100 120	o
NNA	North North Atlantic	North	50 67.5	-70 30	o

Assessing independence

Independence among runs can be assessed by first removing the trend via differencing. Indeed, consider $D_r(t) = \frac{1}{\sqrt{2}}\{T_r(t) - T_{R/2+r}(t)\}$ for $r = 1, \ldots, R/2$. Under the assumption of normality, the dependence is expressed through the covariance matrix among realizations, which is estimated non-parametrically by $\hat{\mathbf{\Sigma}} = \frac{1}{R/2}\sum_{r=1}^{R/2} \mathbf{D}_r \mathbf{D}_r^\top$, where $\mathbf{D}_r = (D_r(1), \ldots, D_r(n))$. Under independence the matrix is diagonal, and tests can be performed to check if the off-diagonal elements are significantly different from zero. In figure S2 we show the L^2 matrix difference between $\hat{\mathbf{\Sigma}}$ and a matrix with only the diagonal entries of the same matrix. The difference is overall small, and in vast areads of the ocean less than 0.05, thus strongly suggesting independence of the runs.

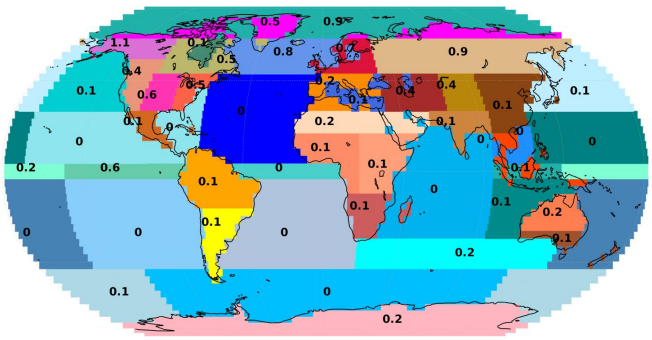

Figure S2: Map of the L^2 norm of the difference between the empirical covariance and the empirical diagonal covariance.

Index of trend

Technical details for inference

Let us denote by $T_r(t)$ the temperature for realization r at time t for a generic region, and by $\mathbf{T}$ the stacked vector of time series across realizations. (We will use the same notation with all the other quantities in this section.)

Model (1) and (2) can be written in vector form as a conditional linear model, i.e..

$$\mathbf{T} = \mathbf{X}(\rho)\boldsymbol{\beta} + \boldsymbol{\varepsilon}, \tag{S1}$$

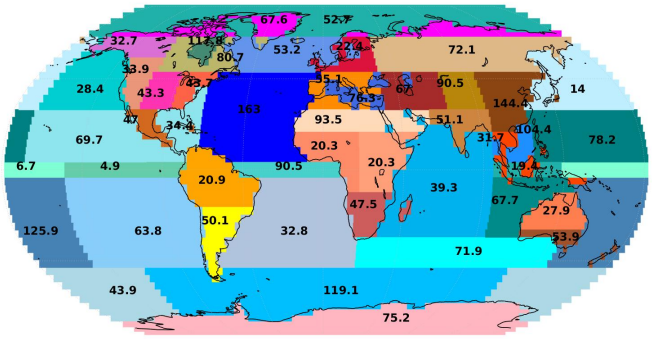

Figure S3: Map of I_{trend} as defined in (4).

where $\boldsymbol{\varepsilon} = (\varepsilon(1), \ldots, \varepsilon(R * n)) \sim \mathcal{N}(\mathbf{0}, \boldsymbol{\Sigma})$ is the random vector with the temporal dependence across realizations, and $\boldsymbol{\Sigma}$ is a block diagonal matrix with R identical blocks of size $n \times n$ representing the temporal dependence, depending on the month specific variance and the autoregressive parameters. Further, $\boldsymbol{\beta} = (\beta_0, \beta_1, \{\gamma_k, \gamma_k', \zeta_k, \zeta_k'\}_{k=1,\ldots,K})$ and $\mathbf{X}(\rho)$ is the design matrix induced by the functional form in (2). While it is possible to estimate $\boldsymbol{\Sigma}, \boldsymbol{\beta}$ and ρ jointly, to simplify the inference we first estimate $\boldsymbol{\Sigma}$ in two steps: fist the month specific variance and then the autoregressive structure.

We consider $D(t) = \frac{1}{\sqrt{2}}\{T_1(t) - T_2(t)\}$, the normalized difference between the first two ensemble members (as there are at least two run in the training set). The month specific variance $\sigma^2_{\text{mn}}, \text{mn} = 1, \ldots, 12$ is estimated by considering all the observations corresponding to the same month and computing the sample standard deviation

$$\hat{\sigma}^2_{\text{mn}} = \frac{1}{n/12} \sum_{i=0}^{n/12-1} D(mn + 12i)^2.$$

We now denote $\tilde{D}(t)$ the vector of $D(t)$ normalized by its corresponding month specific standard deviation. The autoregressive parameters $\boldsymbol{\phi} = (\phi_1, \ldots, \phi_p)$ can then easily estimated via a linear model

$$\tilde{\mathbf{D}} = \tilde{\mathbf{D}}_{\text{lag}}\boldsymbol{\phi} + \boldsymbol{\eta} \implies \hat{\boldsymbol{\phi}} = (\tilde{\mathbf{D}}_{\text{lag}}^\top \tilde{\mathbf{D}}_{\text{lag}})^{-1} \tilde{\mathbf{D}}_{\text{lag}} \tilde{\mathbf{D}}$$

where $\tilde{\mathbf{D}}_{\text{lag}}$ is a design matrix with p columns, each corresponsing to the lagged vector $\tilde{\mathbf{D}}$ with up two p lags, and $\boldsymbol{\eta} \overset{\text{iid}}{\sim} \mathcal{N}(0, \tilde{\sigma}^2\mathbf{I})$ is the white noise.

Once the month specific variance and the autoregressive parameters are estimated, the estimated covariance structure (S1) will be denoted as $\hat{\mathbf{\Sigma}}$. The likelihood can be written as

$$\begin{aligned} \ell(\rho, \boldsymbol{\beta} \mid \mathbf{T}) &= -\tfrac{nR}{2} - \tfrac{1}{2}|\mathbf{\Sigma}| - \tfrac{1}{2}\left\{\mathbf{T} - \mathbf{X}(\rho)\boldsymbol{\beta}\right\}^{\top} \mathbf{\Sigma}^{-1} \left\{\mathbf{T} - \mathbf{X}(\rho)\boldsymbol{\beta}\right\} \\ &\approx -\tfrac{nR}{2} - \tfrac{1}{2}|\hat{\mathbf{\Sigma}}| - \tfrac{1}{2}\left\{\mathbf{T} - \mathbf{X}(\rho)\boldsymbol{\beta}\right\}^{\top} \hat{\mathbf{\Sigma}}^{-1} \left\{\mathbf{T} - \mathbf{X}(\rho)\boldsymbol{\beta}\right\} \end{aligned}$$

Conditionally on ρ, (S1) is a linear model, so the mean can be obtained in closed form with generalized least squares: $\hat{\boldsymbol{\beta}} = \{\mathbf{X}(\rho)^{\top}\hat{\mathbf{\Sigma}}^{-1}\mathbf{X}(\rho)\}^{-1}\mathbf{X}(\rho)\hat{\mathbf{\Sigma}}^{-1}\mathbf{T}$. Therefore, previous expression simplifies in a profile likelihood which only requires to be maximized with respect to ρ.

Gaussianity

Figure S4 shows the diagnostics for Gaussianity of the SG.

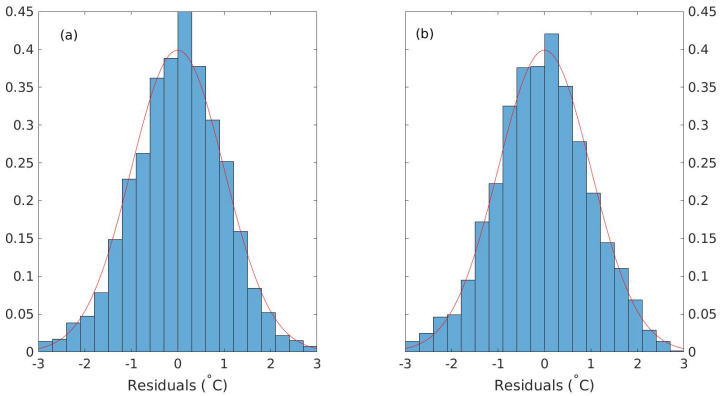

Figure S4: Histogram of residuals of the SG, for (a) Southern Europe and (b) North Atlantic Ocean, overlaid with the probability density function of a normal distribution.

Temporal structure

Figure S5 shows the diagnostics for the temporal structure.

Extrapolation in time

Figure S6 shows the the effects of using a trend model against the SG with a back tracjectory dependence.

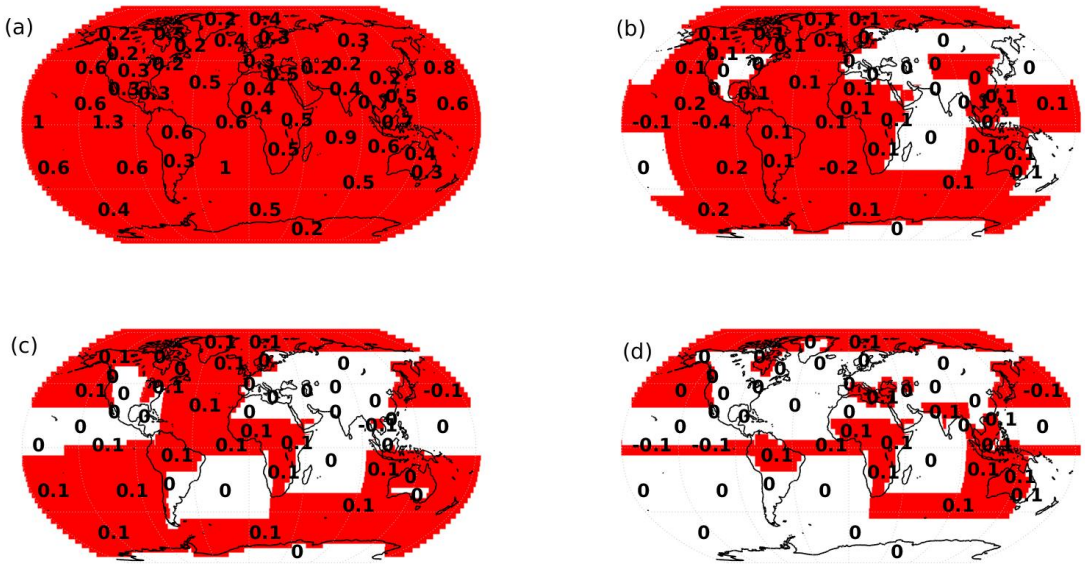

Figure S5: Estimated coefficients for a SG with an AR(4) structure. Red indicates a p-value below the 5% threshold.

Signal-to-noise

Figure S7 shows the median signal-to-noise ratio across the linear parameters of the SG.

Simulating short term events

Figure S8 shows the comparison between three LE runs with three SG runs.

Uncertainty propagation

Conditionally to ρ, ϕ_1 and ϕ_2 the linear parameter estimates are t distributed with closed form expressions for mean and variance. Therefore, it is possible to obtain draws and assess how the uncertainty propagates. Figures S9 and S10 show identical results to figure 4 and 5 in the manuscript for the first two boxplots, but have also a third boxplot with $R = 30$ draws from a SG that accounts for uncertainty propagation, and the plots confirm that uncertainty propagation is not a strong factor, as already observed in Figure S7.

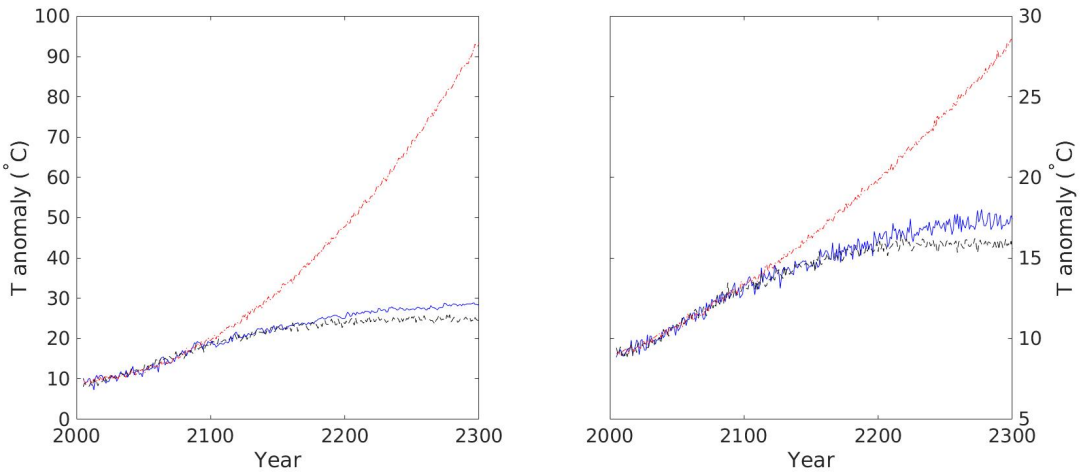

Figure S6: Comparison between a CCSM4 extended run (solid blue), a SG as specified in the manuscript (dashed black), and a SG with no back trajectory dependence on the forcing (dashed and pointed red) for (a) Arctic Ocean and (b) Southern Europe.

Simulating the interannual range

Figure S11 compares the interannual range of LE and SG for two regions.

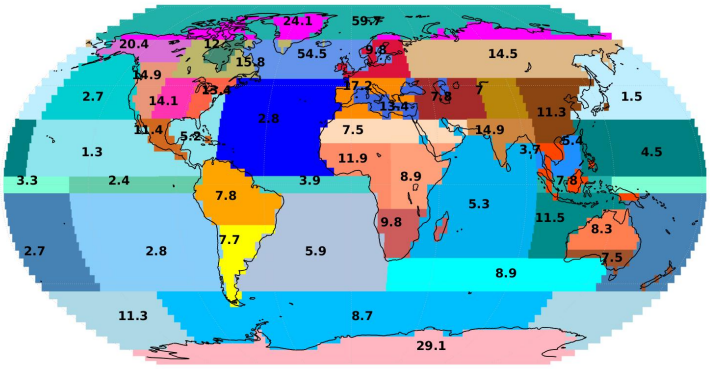

Figure S7: Map of the median signal-to-noise ratio across the linear parameters of the SG.

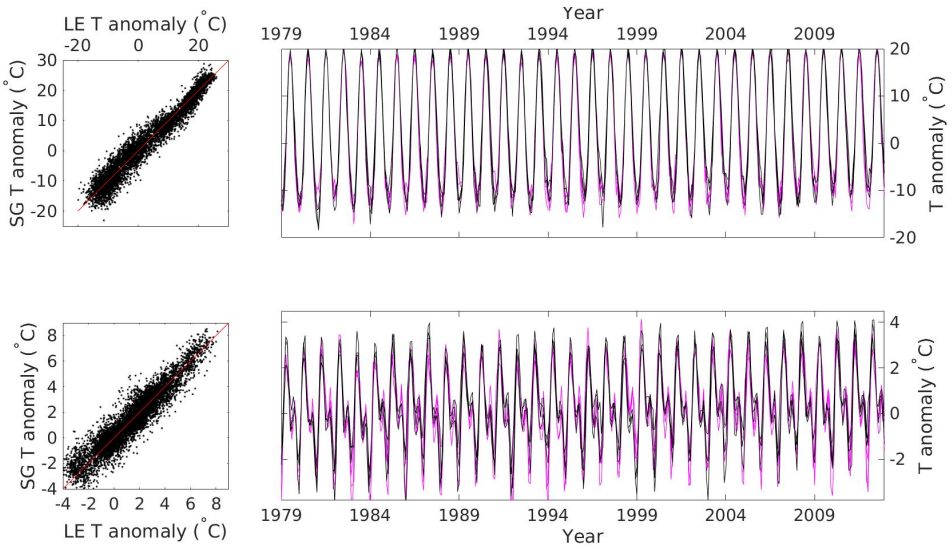

Figure S8: A comparison of three randomly selected runs from the LE (in magenta) against three randomly selected superimposed runs of the SG (in black), for the Artic Ocean (ARO) (left) and the West Africa (WAF) region (right). (a,c) Show the scatterplot of LE against SG data, while (b,d) show the time series for a 34-years reference period (1979–2012) used in the trend analysis.

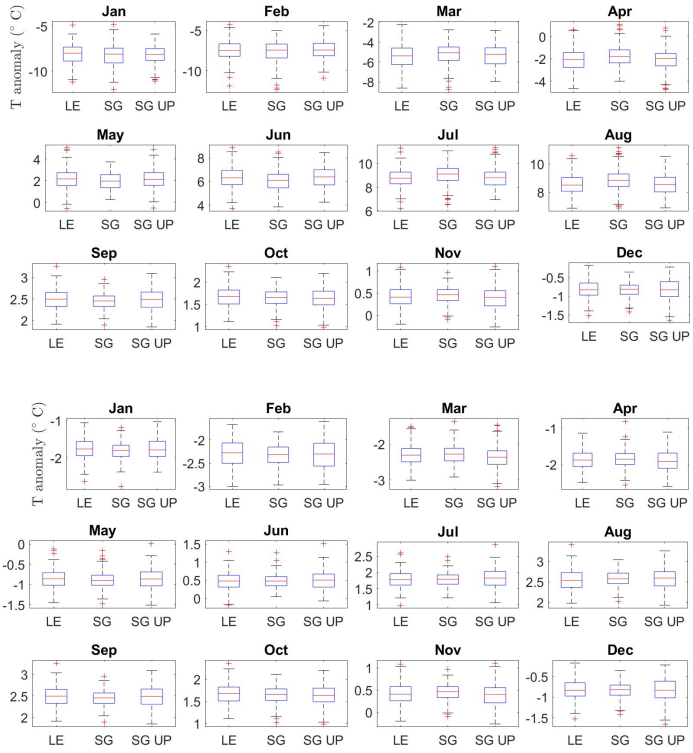

Figure S9: Boxplot comparison of the distribution of temperature for Southern Europe (SEU, top) and North Atlantic (NAT, bottom). Three runs for the large ensemble are considered (left boxplot) from 1920 to 2000 and compared against three runs generated from the statistical model for each month with and without uncertainty propagation.

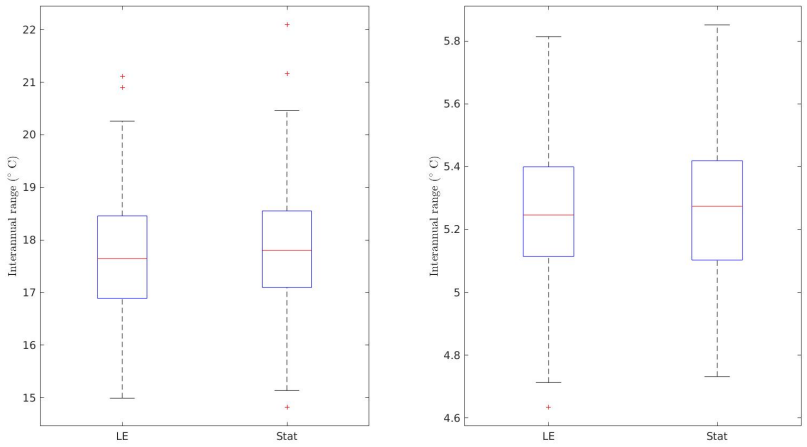

Figure S10: Boxplot of the interannual cycle from 1920 to 2000 for (a) Southern Europe and (b) the North Atlantic.

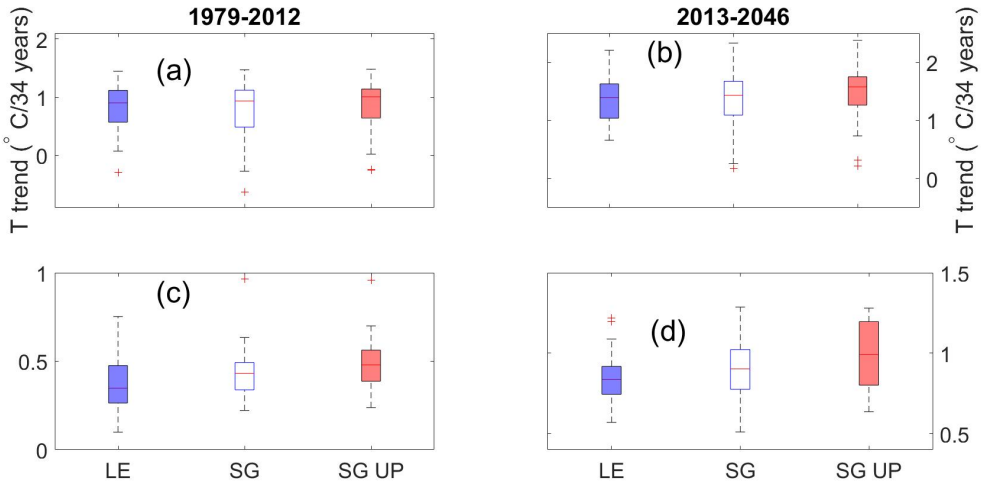

Figure S11: Boreal winter (DJF) surface air temperature trends (°C/34 years) for the 30 LE members (blue boxplots) and 30 simulations generated from the SG (red boxplots). The first row shows the results for Southern Europe (SEU) (a,b) and the second row for the North Atlantic (NAT) (c,d) for the two 34-years reference periods with and without uncertainty propagation.

Realization plots

Figures S12 through S15 show the trend estimates for individual runs/realizations for the LENS and the statistical model, and their corresponding ensemble means and standard deviations.

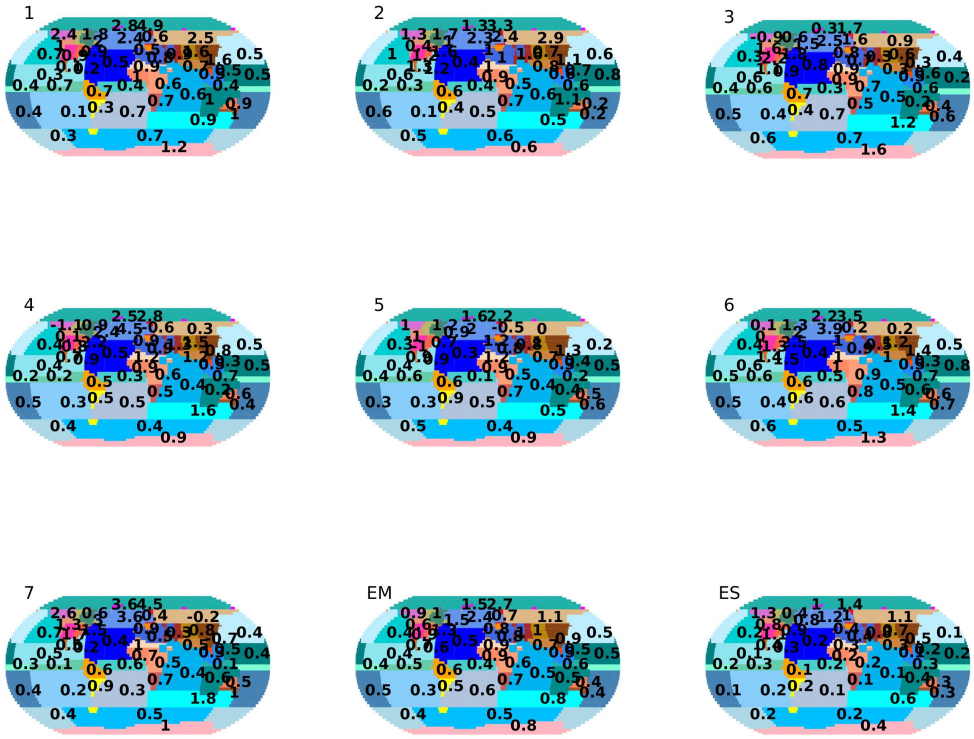

Figure S12: Boreal winter (DJF) surface air temperature trend (°C/34 years) for the first seven ensemble runs, ensemble mean (EM) and ensemble standard deviation (ES) according to LENS for 1979-2012

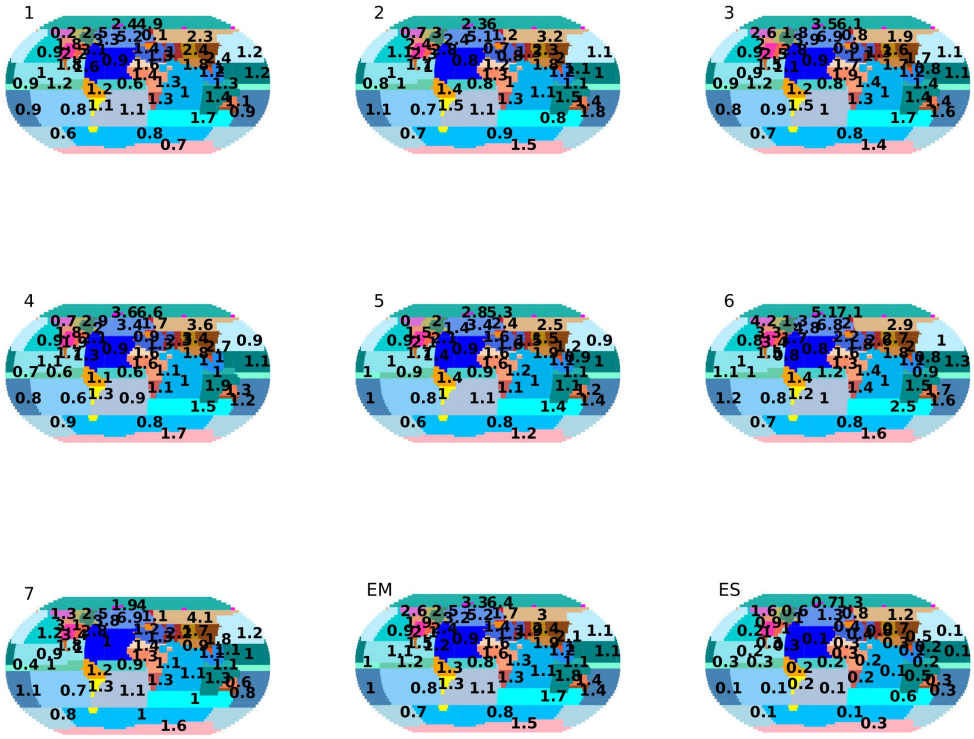

Figure S13: Boreal winter (DJF) surface air temperature trend (°C/34 years) for the first seven ensemble members, ensemble mean (EM) and ensemble standard deviation (ES) according to LENS for 2013-2046

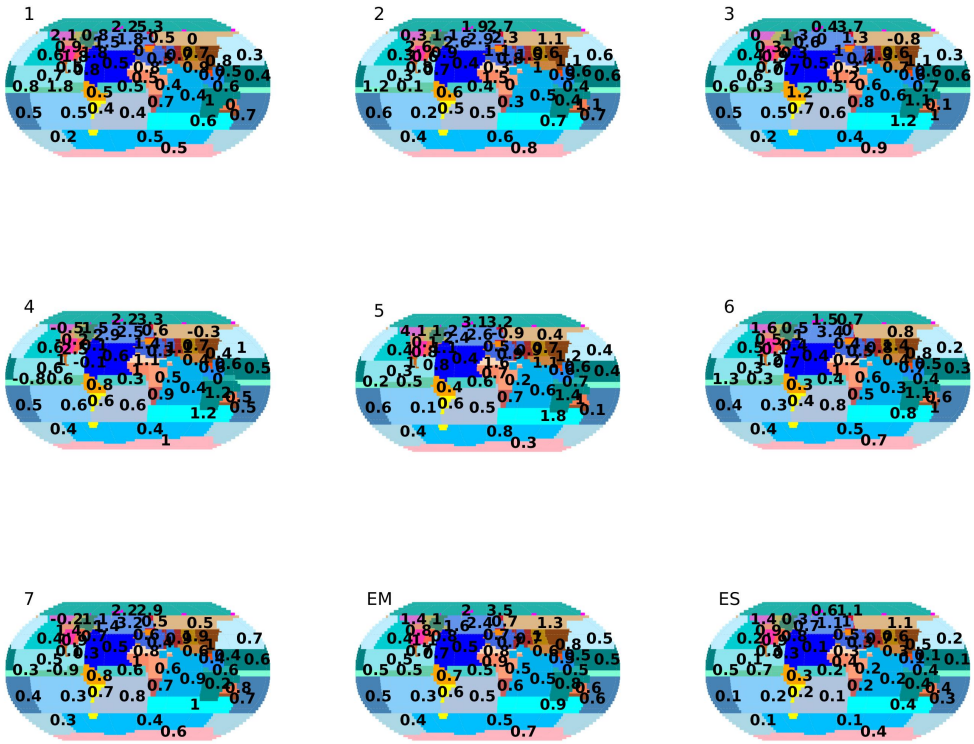

Figure S14: Boreal winter (DJF) surface air temperature trend (°C/34 years) for the first seven realizations, ensemble mean (EM) and ensemble standard deviation (ES) according to the statistical model for 1979-2012

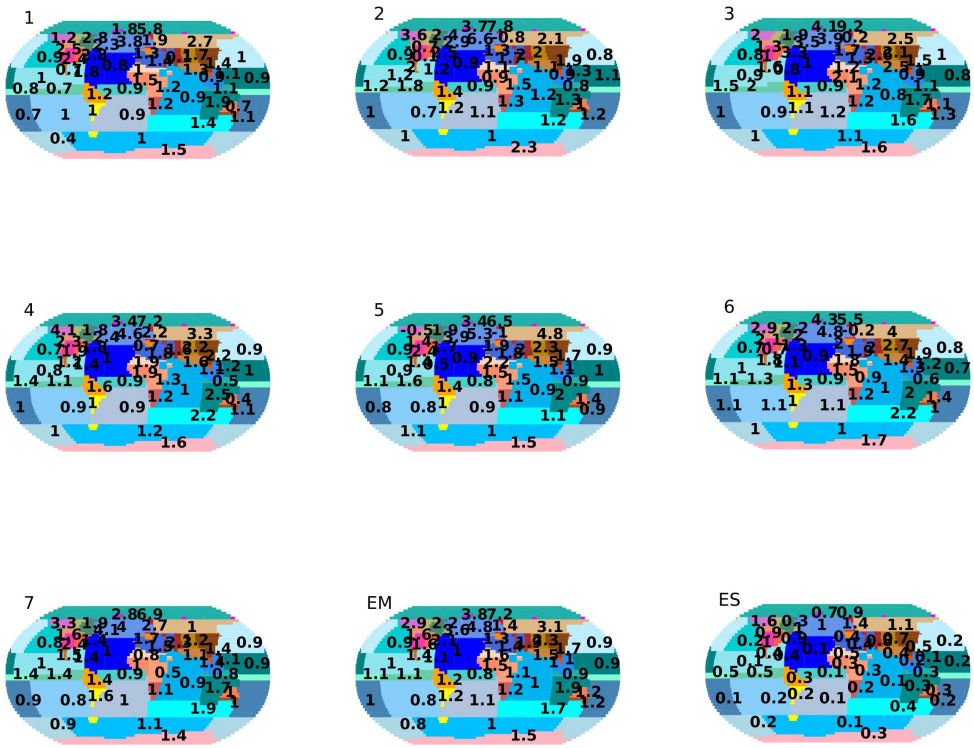

Figure S15: Boreal winter (DJF) surface air temperature trend (°C/34 years) for the first seven simulations, ensemble mean (EM) and ensemble standard deviation (ES) according to the statistical model for 2013-2046

References

[1] S. Castruccio, D.J. McInerney, M.L. Stein, F. Liu, R.L. Jacob, and E.J. Moyer. Statistical emulation of climate model projections based on precomputed gcm runs. *Journal of Climate*, 27:1829–1844, 2014.

[2] Y. Sun and M.G. Genton. Functional boxplots. *Journal of Computational and Graphical Statistics*, 20(2):316–334, 2011.